UV Photolysis Products of Propiolic Acid in Noble-Gas Solids

Esa Isoniemi, Leonid Khriachtchev,* Maarit Makkonen, and Markku Räsänen

Laboratory of Physical Chemistry, P.O. Box 5, University of Helsinki, Helsinki FIN-00014 Finland

Received: April 4, 2006; In Final Form: August 9, 2006

Photolysis (193 nm) of propiolic acid (HCCCOOH) was studied with Fourier transform infrared spectroscopy in noble-gas (Ar, Kr, and Xe) solid matrixes. The photolysis products were assigned using ab initio quantum chemistry calculations. The novel higher-energy conformer of propiolic acid was efficiently formed upon UV irradiation, and it decayed back to the ground-state conformer on a time scale of ∼10 min by tunneling of the hydrogen atom through the torsional energy barrier. In addition, the photolysis produced a number of matrix-isolated 1:1 molecular complexes such as HCCH···CO_2, HCCOH···CO, and H_2O···C_3O. The HCCH···CO_2 complex dominated among the photolysis products, and the computations suggested a parallel geometry of this complex characterized by an interaction energy of −9.6 kJ/mol. The HCCOH···CO complex also formed efficiently, but its concentration was strongly limited by its light-induced decomposition. In this complex, the most probable geometry was found to feature the interaction of carbon monoxide with the OH group via the carbon atom, and the computational interaction energy was determined to be −18.3 kJ/mol. The formation of the strong H_2O···C_3O complex (interaction energy −21 kJ/mol) was less efficient, which might be due to the inefficiency of the involved radical reaction.

Introduction

Photodissociation of small molecules in noble-gas solids is a fundamentally and practically important topic that has attracted a great deal of attention.[1] Many examples exist in which solid-phase photolysis products are essentially different from the corresponding gas-phase products, as a result of the well-known cage effect. Carboxylic acids provide an intriguing example of solid-state photolysis. Formic acid (HCOOH) is decomposed by UV light in solid hosts to the H_2 + CO_2 and H_2O + CO products.[2,3] Acetic acid (CH_3COOH) photodecomposes into a number of molecular complexes, and the major photolysis channel leads to a complex of methanol and carbon monoxide produced by radical reactions in the primary photolysis.[4] Thus, photolysis in solid hosts allows various 1:1 complexes to be isolated in large amounts, which is practically impossible to achieve through deposition of a gas-phase mixture of the precursors.

Another topic of interest in the photochemistry of small molecules in noble-gas solids is the preparation of various rotational isomers (conformers). The less stable conformers can be formed upon UV or IR (broad or narrowband) irradiation.[3−11] The quantum yield of the IR-induced isomerization can be very high, and this makes novel reactive vibrational excitation spectroscopy possible.[10] It has been found that the stability of the higher-energy conformers of small carboxylic acids (formic, acetic, and propionic) is limited by proton tunneling, and this process is surprisingly host-dependent.[11] The tunneling rate also depends on the conformational energy barrier and the vibrational density of states of the final species at the energy of the unstable form.[9]

The vibrational spectra in the liquid phase and in Ar, CO, and N_2 matrixes of the ground-state conformer of propiolic acid (HCCCOOH, acetylenecarboxylic acid, propynoic acid, 2-propynoic acid, carboxyacetylene, propargylic acid), another representative of small carboxylic acid, have been reported.[12,13] Upon 193-nm irradiation in the gas phase, propiolic acid produces in a good yield OH radicals, but a number of other channels are also energetically possible.[14] The decomposition channels of propiolic acid in the ground electronic state, which produce acetylene + carbon dioxide and ethynol + carbon monoxide, have been studied theoretically.[15] In the gas phase, acetylene and carbon dioxide form a van der Waals complex in which the molecules are in a parallel configuration.[16−18] The IR absorption spectra of ethynol, another possible decomposition product, have been characterized both experimentally in Ar matrixes[19,20] and computationally.[21,22] The higher-energy conformer and solid-phase photolysis of propiolic acid have not been experimentally investigated to the best of our knowledge.

In the present work, we studied the 193-nm photolysis of propiolic acid in Ar, Kr, and Xe matrixes. One of the photolysis products is a novel higher-energy rotational isomer. In addition, photolysis of propiolic acid produces molecular complexes of acetylene and carbon dioxide (HCCH···CO_2), ethynol and carbon monoxide (HCCOH···CO), and water and tricarbon monoxide (H_2O···C_3O). The IR absorption spectra of these photolysis products were characterized experimentally and using ab initio calculations.

Experimental and Computational Details

Gaseous mixtures of propiolic acid (PA) with noble gases (typically PA/Ng ≈ 1:1000; Ng = Ar, Kr, and Xe) were prepared. We used the following gases: propiolic acid (99.85%, Merck), Ar (99.9999%, Aga), Kr (99.997%, Aga), and Xe (99.997%, Aga). The gas mixtures were deposited onto a cold CsI substrate in a closed-cycle helium cryostat (DE-202A, APD), at deposition temperatures of 10−20, 20−25, and 30−35 K for Ar, Kr, and Xe samples, respectively. The typical matrix thickness was 100 μm. An MPB MSX-250 excimer laser operating at 193 nm with a pulse energy density of ∼10 mJ/cm^2 was employed for photolysis. The IR absorption spectra

* To whom correspondence should be addressed. E-mail: leonid.khriachtchev@helsinki.fi.

10.1021/jp062080k CCC: $33.50
Published on Web 09/21/2006

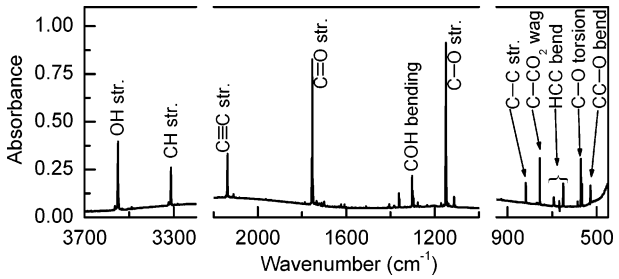

Figure 1. IR absorption spectrum of *t*-PA in solid Ar at 9 K. The fundamental modes are marked.

were measured with a Nicolet 60SX FTIR spectrometer with 1 cm^{-1} resolution.

The Gaussian 98 program was employed for the geometry optimizations and harmonic vibrational calculations, and the torsional potential energy barriers were obtained with the Gaussian 03 program.[23] Electron correlation was considered via Møller−Plesset perturbation theory to the second order (MP2). The split-valence, triple-ζ, 6-311G-type Gaussian basis set, including multiple sets of diffuse and polarization functions [6-311++G(2d,2p)], was used for all atoms. The calculations were carried out on an SGI Origin 2000 computer at CSC—Scientific Computing Ltd. (Espoo, Finland). The interaction energies of the complexes did not include basis set corrections. The energy barriers and energy differences of the conformers are presented after correction for the zero-point vibrational energies.

Results and Assignment

1. *trans*-Propiolic Acid. Figure 1 shows the spectrum of as-deposited propiolic acid in an Ar matrix at 9 K, featuring the absorption bands of the ground-state trans conformer of propiolic acid (*t*-PA). It should be noted that we use different nomenclature from refs 14 and 15 and call the ground state form the trans conformer, following the nomenclature previously used for formic, acetic, and propionic acids.[3,4,8−11] The deposited samples are quite monomeric with respect to propiolic acid, and natural matrix impurities (water and air) are minor. All fundamental absorptions of *t*-PA are observed in our experimental spectral region. The absorption frequencies of *t*-PA in Ar, Kr, and Xe matrixes are collected in Table 1. The calculated vibrational spectrum of *t*-PA is in complete agreement with the experimental data, as in the previously studied cases of formic, acetic, and propionic acids.[8−11] The calculated intensities also correlate with the measured absorption intensities. On the basis of the calculated spectrum, the experimental absorption bands of *t*-PA were assigned as shown in Table 1.

Under irradiation at 193 nm, the IR absorption bands of *t*-PA decreased, and four new sets of absorption bands appeared. These sets of bands were assigned to the higher-energy cis conformer of propiolic acid and to the molecular complexes between acetylene and carbon dioxide, ethynol and carbon monoxide, and water and tricarbon monoxide, as described below.

2. *cis*-Propiolic Acid. Photolysis at 193 nm of the as-deposited sample produced a group of absorption bands featuring characteristics similar to those of *t*-PA. On the basis of our experience with the IR absorption spectra of other carboxylic acids, we assigned these bands experimentally to the higher-energy cis conformer of propiolic acid (*c*-PA). The experimental absorptions of *c*-PA in various matrixes are collected in Table 2. As the best fingerprint, the trans and cis conformers can be recognized from the characteristic shifts of the C═O and O—H stretching modes. For the cis form, the O—H and C═O stretching frequencies increase (see Figure 2), as observed previously for formic, acetic and propionic acids.[9]

The conformers of propiolic acid were studied computationally (see Figure 3). Computationally, the trans form is 12.2 kJ mol^{-1} (1020 cm^{-1}) lower in energy than *c*-PA, and the conformers are separated by a trans-to-cis barrier of 3742 cm^{-1}. In reasonable agreement, Kumar et al. obtained values of 1365 cm^{-1} for the energy difference (MP2) and 3990 cm^{-1} for the barrier.[14] The H—C≡C—C group is nearly linear in both conformers. The dipole moment of the cis conformer (∼4.9 D) is considerably larger than the 1.9-D dipole moment of the trans conformer, in qualitative agreement with the results for other carboxylic acids. The calculated and experimental spectral data for the cis and trans conformers are presented in Tables 1 and 2, and they are in good agreement. For example, the experimental O—H stretching frequencies of the cis and trans conformers differ by 49.4 cm^{-1} in solid Ar, whereas the calculations predict a difference of 50.9 cm^{-1}.

It was experimentally observed that *c*-PA is not stable and its concentration slowly decreases in the dark, whereas the absorptions of *t*-PA simultaneously increase. In Figure 2, the cis-to-trans conversion is demonstrated in solid Ar at 9 K for the characteristic spectral regions. The process presumably occurs via proton tunneling through the torsional barrier, which is similar to the process observed for the other carboxylic acids studied previously.[9] The lifetime of *c*-PA (decay to the 1/e level) is about 400 s in solid Ar at 9 K, i.e., comparable to that of formic acid and considerably longer than those of acetic and propionic acids.[9] In general agreement with these experimental results, the cis−trans barrier calculated for propiolic acid (2722 cm^{-1}) is higher than the computational barriers for acetic (2308 cm^{-1}) and pronionic (2290 cm^{-1}) acids and quite similar to the value for formic acid (2676 cm^{-1}).[9]

3. Complex of Acetylene and Carbon Dioxide. The second set of bands presented in Figure 4 and Table 3 indicates the HCCH···CO_2 complex. The rising absorption bands are close to the stretching and bending absorptions of the C_2H_2 and CO_2 monomers. The C—H stretching bands of acetylene in the complex form are shifted from the monomeric bands by 0.3 and −3.3 cm^{-1} in solid Ar, and the bending mode is shifted by 1.2 cm^{-1}; similarly small shifts are observed in the Kr and Xe matrixes.[24,25] In solid Ar, we observed two stretching absorption bands of CO_2 at 2344.0 (the main band) and 2340.8 cm^{-1} (the weak band), as well as the bending absorptions at 663.2 and 656.1 cm^{-1}, meaning that the complexation-induced shifts were quite small.[26,27] The weak band at 2340.8 cm^{-1} for the CO_2 stretching absorption is probably due to matrix-site effects, as is the case for the monomer.

Several geometries of the HCCH···CO_2 complex were studied computationally, and two structures were found to correspond to the true energy minima (see Figure 5). These parallel and linear complex geometries are characterized by interaction energies of −9.6 and −6.7 kJ/mol, respectively, i.e., the parallel complex geometry is lower in energy by 2.9 kJ/mol. The acetylene and carbon dioxide molecules are practically linear in both geometries. The vibrational frequencies for the linear and parallel complexes and the corresponding monomers are included in Table 3. The present calculations agree with the results of earlier ab initio studies for this system.[17] In the parallel complex geometry, the calculated shift for the HCCH bending mode is 3.3 and −1.0 cm^{-1}, which agrees well with the experimentally observed value of a few cm^{-1}, whereas the calculated shift is considerably larger (24.4 cm^{-1}) in the

TABLE 1: Experimental and Computational IR Absorption Spectral Data (in cm^{-1}) for *trans*-Propiolic Acid[a]

mode	Ar	Kr	Xe	calcd	Ar[b]
O—H stretch	3550.8 (0.332)	3537.6	3525.0	3774.0 (110)	3550.0
C—H stretch	3313.1 (0.158)	3305.4	3304.7	3475.6 (57)	3315.6
C≡C stretch	2137.3 (0.167)	2133.9	2132.4	2133.7 (59)	2140.0
C═O stretch	1753.9 (0.793)	1749.4	1744.5	1764.4 (314)	1753.7
COH bend	1302.2 (0.194)	1299.1	1296.4	1364.3 (82)	1303.0
C—O stretch	1149.5 (0.695)	1146.2	1143.0	1169.2 (398)	1151.0
C—C stretch	818.1 (0.063)	816.0	814.9	818.8 (25)	817.5
C—CO_2 wag/ OCO out-of-plane bend	755.0 (0.152)	753.5	752.3	767.5 (50)	755.2
HCC out-of-plane bend	692.8 (0.050)	690.9	696.0 689.3	679.8 (29)	695.1
HCC in-plane bend	650.3 (0.087)	647.9	648.0	662.1 (35)	653.1
COH torsion	571.3 566.6 (0.251)	569.1 565.0	567.6 563.3	607.3 (86)	587.5
CC═O in-plane bend	585.8 (0.016)	584.2	584.3	583.2 (5)	572.4
CC—O bend/OCO scissor	528.4 (0.059)	527.2	526.0	525.2 (22)	529.5
HCCC out-of-plane bend	–	–	–	245.3 (8)	–
HCCC in-plane bend	–	–	–	168.2 (5)	–

[a] Experimental intensities in solid Ar shown in parentheses are relative, and calculated intensities are in kJ/mol. The ab initio spectrum was calculated at the MP2/6-311++G(2d,2p) level. [b] Data from ref 13.

TABLE 2: Experimental and Computational IR Absorption Spectral Data (in cm^{-1}) for *cis*-Propiolic Acid[a]

					$\omega_{cis} - \omega_{trans}$	
mode	Ar	Kr	Xe	calcd	Ar	calcd
O—H stretch	3600.2 (0.059)	3581.2	3554.9	3824.9 (83)	49.4	50.9
C—H stretch	3308.9 (0.042)	3301.0	3301.4	3470.9 (61)	−4.2	−4.7
C≡C stretch	2127.1 (0.034)	2121.1	2123	2112.1 (46)	−10.2	−21.6
C═O stretch	1787.4 (0.182)	1781.8	1775.6	1796.2 (262)	33.5	31.8
COH bend	1287.1 (0.256)	1286.7	1284.4	1311.0 (443)	−15.1	−53.3
C—O stretch	1157.7 (0.011)	1156.8		1174.5 (83)	8.2	5.3
C—C stretch	826.8 (0.018)	825.7	824.9	825.2 (31)	8.7	6.4
C—CO_2 wag	743.9 (0.026)	743.1	742.2	752.0 (15)	−11.1	−15.5
HCC out-of-plane bend	689.3 (0.023)	688.4	686.1	675.7 (34)	−3.5	−4.1
HCC in-plane bend	655.4 (0.019)	653.0	652.3	664.6 (37)	5.1	2.5
CC═O bend/ CCC in-plane bend	588.9 (0.006)	588.4	–	586.1 (9)	3.1	2.9
CC—O bend/OCO scissor	–	–	–	537.7 (4)	–	12.5
COH torsion	477.9 (0.079) 475.5	475.5 472.4	473.9 470.3	495.3 (114)	−93.4 −91.0	−112.0
HCCC out-of-plane bend	–	–	–	242.1 (<1)	–	−3.2
HCCC in-plane bend	–	–	–	164.9 (3)	–	−3.3

[a] Absorption intensities are in parentheses (calculated values are in kJ/mol). The ab initio spectrum was calculated at the MP2/6-311++G(2d,2p) level.

linear complex geometry. The experimental splitting of the OCO bending mode (7.1 cm^{-1} in Ar) also supports the parallel complex geometry (calculated splitting of 11.8 cm^{-1} with a proper intensity ratio), as no splitting should be seen in the linear complex because of its symmetry. For the stretching modes, the linear and parallel geometries exhibit similar shifts and intensities. The 4.3 cm^{-1} splitting of the bending mode of acetylene predicted for the parallel geometry is not observed experimentally; however, the experimental full width at half-maximum of this band is 2.6 cm^{-1}, which can be a result of two overlapping absorptions with similar intensities. Thus, the lower-energy parallel complex geometry is the most probable experimental structure.

4. Complex of Ethynol and Carbon Monoxide. The third set of absorption bands formed upon the photolysis of propiolic acid was assigned to the complex of ethynol (HCCOH) and carbon monoxide (see Figure 6 and Table 4). The observed absorptions are close to the known spectra of the ethynol (O—H, C—H, and C≡C stretching modes) and carbon monoxide monomers.[19−20,28] These bands are extensively split in the Ar and Kr matrixes, whereas only single bands are seen in solid Xe; this is consistent with matrix-site effects.

For this complex, two minimum-energy structures were found computationally in which the C atom of CO interacts with acetylene, as shown in Figure 7. The complex structures in which terminal H atoms interact with the oxygen atoms of CO were found to be transition states. The calculated interaction energies in the HCCOH···CO and OC···HCCOH geometries are −18.3 and −6.4 kJ/mol, respectively, i.e., the OH-bonded species is much more stable. The interaction of CO with the OH group (HCCOH···CO structure) is calculated to shift the O—H stretching band by −131.7 cm^{-1} from the monomeric value, whereas the binding of CO to the acetylene group (OC···HCCOH structure) shifts the O—H stretching band by 1.5 cm^{-1}. In the present experiments, the O—H stretching absorptions of HCCOH appear in the 3475−3510 cm^{-1} region in solid Ar, i.e., they are shifted down in energy by 80−113 cm^{-1} from the monomeric position at 3588.2 cm^{-1}.[20] This experimental shift agrees with the computation for the HCCOH···CO complex geometry. The higher-energy doublet in solid Ar (site 2) is close to the 3501.3 cm^{-1} absorption reported in ref 19 for the HCCOH···CO complex. Actually, the literature value might correspond to the complex of ethynol with two CO molecules, which would agree with the reported synthesis method.[19] Our

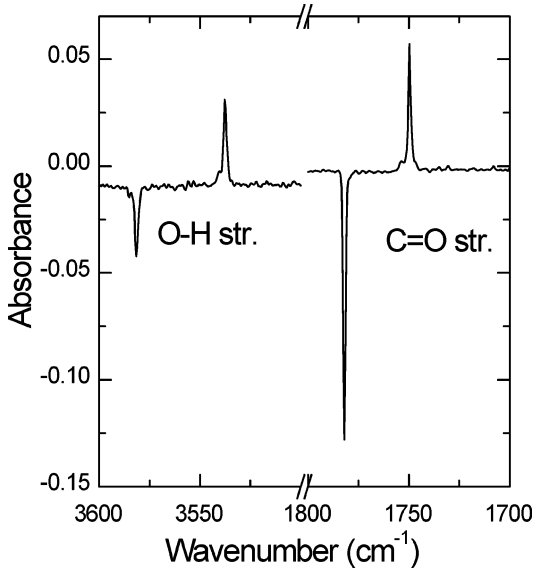

Figure 2. IR absorption spectrum demonstrating dark conversion of *c*-PA to *t*-PA after 193-nm irradiation in solid Ar at 9 K. The characteristic O—H and C═O stretching absorption bands are shown. The increasing bands arise from the trans conformer, and the decreasing absorptions originate from the decaying cis conformer.

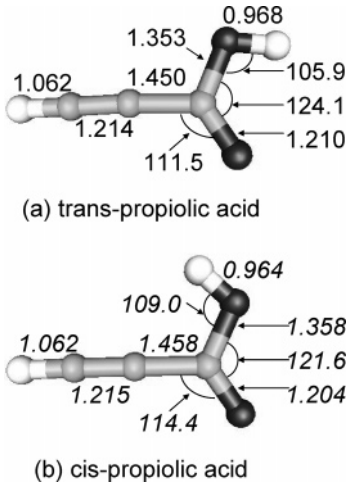

Figure 3. Calculated structures of (a) *trans*- and (b) *cis*-propiolic acid. The bond lengths are in angstroms, and the angles are in degrees. The geometries were calculated at the MP2 level of theory with the 6-311++G(2d,2p) basis set.

experimental spectra provide no evidence for the weakly bound OC···HCCOH complex geometry. The absorption band of the free O—H stretching mode of this structure should be close to the monomeric position at ~3590 cm^{-1}, which is not observed experimentally; however, such a band might be overlapped by the absorptions of *t*-PA, *c*-PA, and $H_2O···C_3O$. The detection of this structure in the O—H stretching region is further complicated by the relative weakness of its absorption (computationally 144 kJ/mol compared to 625 kJ/mol for the other structure) and the small concentration of this complex (see later).

According to our calculations, the C—H stretching mode is shifted by −22.3 cm^{-1} in the OC···HCCOH complex geometry, whereas practically no shift is predicted for the HCCOH···CO complex. Experimentally, the C—H stretching absorptions are at 3362.0 and 3344.7 cm^{-1} in solid Ar, giving shifts of 16.8 and −0.5 cm^{-1}, respectively, from the corresponding bands of the monomer.[20] In this situation, the OC···HCCOH structure has no support because of the calculated red shift. Following the normal matrix shift from Ar to Kr and to Xe, the higher-energy absorption with the large blue shift is assigned to site 1. This large blue shift is not predicted computationally, which might be an indication of a misinterpretation of the C—H stretching mode for monomeric ethynol.[20]

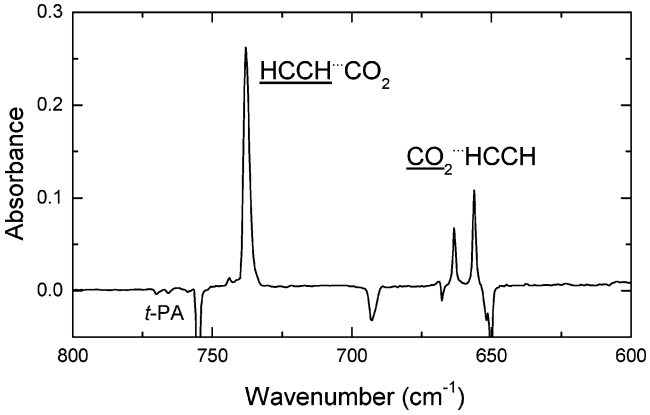

Figure 4. IR absorption spectrum of the $H_2C_2···CO_2$ complex in the bending region in solid Ar at 9 K. The absorbing molecules are underlined. In the difference spectrum, the negative absorption bands arise from decomposed *t*-PA.

With respect to the C≡C stretching mode, the computational shifts are −5.7 and −3.6 cm^{-1} for the HCCOH···CO and OC···HCCOH complex geometries, respectively. The experimental shifts are 5.7 and −3.7 cm^{-1} in solid Ar, which disagrees with the calculations with respect to the higher-energy band. Assuming normal matrix shifts, the higher-energy C≡C stretching bands at 2207.8 and 2205.7 cm^{-1} in solid Ar and Kr, respectively, are assigned to site 1, and the lower-energy absorptions at 2198.4 and 2197.0 cm^{-1} to site 2. In solid Xe, the single absorption at 2200.1 cm^{-1} belongs to site 1.

For carbon monoxide, the computationally predicted shifts are 24.1 and 4.5 cm^{-1} for the HCCOH···CO and OC···HCCOH complex geometries, respectively. The experimentally observed bands are shifted from the monomeric position by 11.8 and 3.0 cm^{-1} in solid Ar, in agreement with the calculations. However, we cannot assign the observed strong CO absorption bands to the complex in question. It is seen in Figure 6 that the CO bands are much stronger than the C≡C, C—H, and O—H stretching bands of HCCOH. The calculations give quite the opposite intensity ratios. This means that the observed CO bands mostly arise from secondary photolysis products, with a probable contribution of impurities. For example, ethynol (HCCOH) is converted to ketene (H_2CCO) by irradiation at wavelengths below 248 nm.[20] The major products of the 193-nm photolysis of ketene are CH_2 + CO and HCCO + H in a 1:3 proportion.[29] This leads to further in-cage reactions, thus decreasing the amount of ethynol with respect to carbon monoxide. For 193-nm photolysis of acetic acid, the CO band at 2152 cm^{-1} was assigned to the primary product ($CO···CH_3OH$) whereas the band at 2140 cm^{-1} was assigned to the CO dimer.[4] In the present study, CO dimers might originate from photolysis of ketene trapped in the same cage with CO molecule.

Thus, the absorptions of the complex between ethynol and carbon monoxide most probably arise from matrix sites of the HCCOH···CO complex geometry in which carbon monoxide is bonded to the OH group via the carbon atom. The suggested assignment is reasonable because the other calculated complex structure has a quite small binding energy. The agreement between experiment and theory is good for site 2, which mainly applies to Ar matrixes. On the other hand, site 1 dominates in

TABLE 3: Experimental and Computational IR Absorption Spectral Data (cm^{-1}) for the $H_2C_2\cdots CO_2$ Complex[a]

	Ar matrix			calcd			calcd shift	
mode	complex	monomers[b]	shift	linear	parallel	monomers	linear	parallel
C—H stretch	3302.8	3302.5	0.3	3441.6 (168)	3443.7 (96)	3445.8 (92)	−4.2	−2.1
	3285.6	3288.9	−3.3					
HCC bend	738.1	736.9	1.2	763.3 (97)	742.2 (94)	738.9 (100)	24.4	3.3
					737.9 (104)			−1.0
C═O stretch	2344.0[c]	2345.0	−1.0	2404.7 (681)	2404.2 (486)	2403.0 (587)	1.7	1.2
		2339.1	4.9					
OCO bend	663.2	663.4	−0.2	663.8 (19)	665.7 (17)	665.6 (22)	−1.8	0.1
	656.1	661.9	−5.8		653.9 (35)			−11.7

[a] Vibrational frequencies are in cm^{-1}, and absorption intensities are shown in parentheses (calculated values are in kJ/mol). The ab initio spectrum was calculated at the MP2/6-311++G(2d,2p) level of theory. [b] Data from refs 24−27. [c] Strongest component.

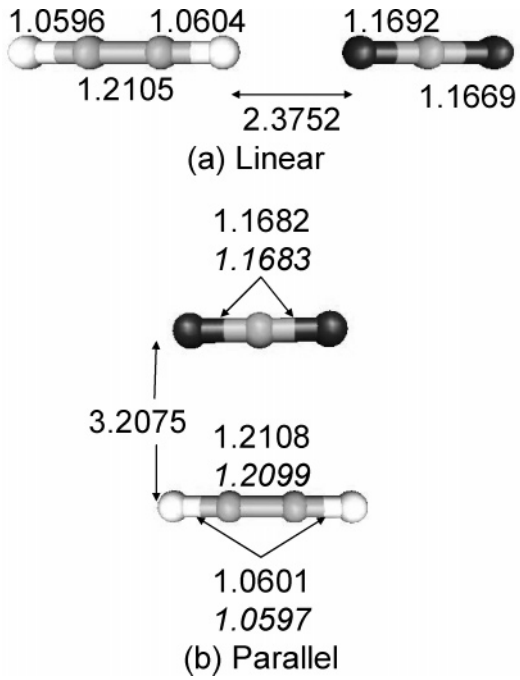

Figure 5. Calculated structures of (a) linear and (b) parallel $H_2C_2\cdots CO_2$ complex. The distances for the complex are shown in normal font, and the values for the corresponding monomers are given in italics (the lower numbers). The geometries were calculated at the MP2 level of theory with the 6-311++G(2d,2p) basis set.

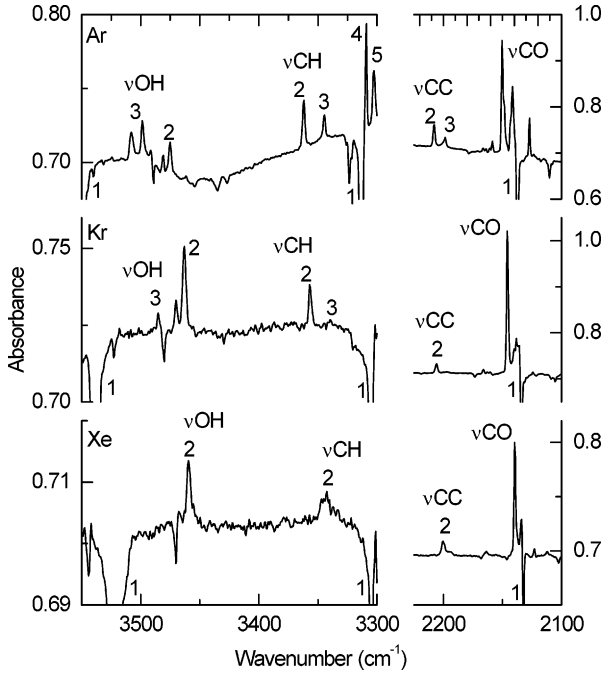

Figure 6. IR absorption spectra of the complex between ethynol and carbon monoxide in solid Ar, Kr, and Xe at 9 K. The decreasing absorption bands arise from *t*-Pa (marked as 1), and the rising bands are the photolysis products: (2 and 3) two sites of HCCOH···CO, (4) *c*-PA, and (5) $HCCH\cdots CO_2$. The bands of CO mostly originate from secondary photolysis channels.

Xe matrixes, and it exhibits worse agreement with the calculations. The reason for this partial discrepancy is unclear at the moment.

5. Complex of Water and C_3O. The fourth set of absorption bands formed upon irradiation of propiolic acid in solid matrixes is assigned to a novel complex of water and tricarbon monoxide (see Figure 8 and Table 5). The absorption bands at 3704.4 and 3598.5 cm^{-1} (in Ar) arising upon photolysis correspond to the O—H stretching (ν_3 and ν_1) modes of water. With respect to the band centers of H_2O monomer,[30] the shifts of the ν_3 and ν_1 modes are −29.9 and −39.5 cm^{-1} in an Ar matrix. The other molecule in the complex is C_3O, which is formed by the elimination of a water molecule from propiolic acid. The strongest absorption of the C_3O monomer is at 2243 cm^{-1} in solid Ar and at 2237.2 cm^{-1} in solid Xe.[31−33] In our experiments, a number of bands appear close to this position (2248.2, 2245.9, and 2243.1 cm^{-1} in solid Ar). The splitting of this absorption probably originates from the matrix-site effect, because annealing at 30 K changes the intensity distribution. The strongest band shows complexation-induced shifts of 2.9 and 2.6 cm^{-1} in the Ar and Xe matrixes, respectively.

In the calculations, only one minimum-energy structure was found for the $C_3O\cdots H_2O$ complex (see Figure 9), with an interaction energy of −21 kJ/mol. The predicted complexation-induced shifts are −35.7 and −116.4 cm^{-1} for the ν_3 and ν_1 modes and 29.4 cm^{-1} for the ν_2 mode of water. The calculated shift for the ν_3 mode corresponds well to the experimental value, whereas the shift for the ν_1 mode is computationally overestimated. The relative intensity of the ν_1 mode is also computationally overestimated. The stretching mode of the complexed C_3O molecule is calculated to be shifted by 2.7 cm^{-1}, in perfect agreement with the experimental data.

The vibrational spectrum of the $H_2O\cdots C_3O$ complex can be compared with those of other relevant complexes. Similar shifts are observed for water dimers in Ar, Kr, and Xe matrixes.[30,34] For example, the O—H stretching frequencies of water dimer donor are 3708.2 and 3573.6 cm^{-1}, giving complexation shifts of −26.1 and −64.4 cm^{-1} in solid Ar, respectively, whereas the bending mode shifts by 21.5 cm^{-1}. In the $H_2O\cdots O$ complex, smaller shifts of the stretching modes were reported (−4.2 and −5.0 cm^{-1}, respectively, for the ν_3 and ν_1 modes in solid Ar), and the bending absorption was not observed, similarly to the present case.[35,36] For the $H_2O\cdots CO$[37] and $H_2O\cdots N_2$[30] complexes in solid Ar, the observed shifts for the ν_3 and ν_1 modes are also small, −8.8 and −9.5 cm^{-1} and −3.1 and −2.1 cm^{-1},

TABLE 4: Experimental and Computational IR Spectral Data (in cm^{-1}) for the Complex between Ethynol and Carbon Monoxide[a]

	Ar matrix			calcd		
mode	complex	monomers[b]	shift	HCCOH···CO	OC···HCCOH	monomer
O−H stretch						
site 2	3508.0	3588.2 (70)	−80.2	3719.8 (625)	3853.0 (144)	3851.5 (145)
	3498.4		−89. 8	[−131.7]	[1.5]	
site 1	3481.0		−107.2			
	3475.2		−113.0			
C−H stretch						
site 1	3362.0	3345.2 (75)	16.8	3510.7 (98)	3488.4 (189)	3510.7 (90)
				[0.0]	[−22.3]	
site 2	3344.7		−0.5			
C≡C stretch						
site 1	2207.8	2202.1 (80)	5.7	2205.6 (170)	2207.7 (117)	2211.3 (137)
				[−5.7]	[−3.6]	
site 2	2198.4		−3.7			
C−O stretch						
site 1	2150.3[c]	2138.5	11.8[c]	2143.8 (26)	2124.2 (38)	2119.7 (36)
				[24.1]	[4.5]	
site 2	2141.5[c]		3.0[c]			

[a] Relative absorption intensities are in parentheses (computational values in kJ/mol). The ab initio spectrum was calculated at MP2/6-311++G(2d,2p). The calculated complexation-induced shifts are in brackets. [b] Data from refs 20 and 28. [c] These bands of CO are probably for another complex.

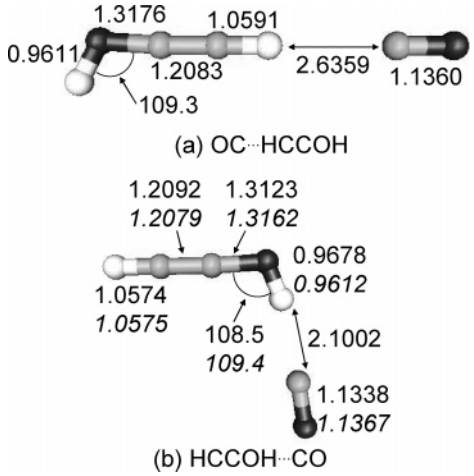

Figure 7. Calculated structures of the complex between ethynol and carbon monoxide: (a) OC···HCCOH geometry and (b) HCCOH···CO geometry. The bond lengths and angles of the complexes are shown in normal font, and the values for the corresponding monomers are given in italics (the lower numbers). The geometries were calculated at the MP2 level of theory with the 6-311++G(2d,2p) basis set.

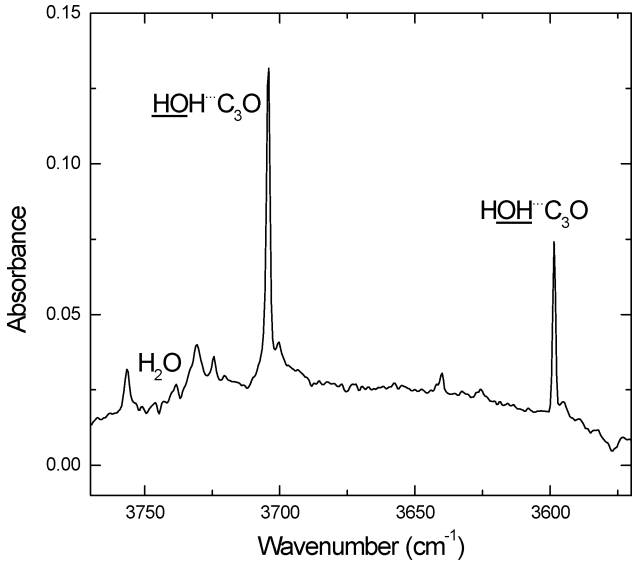

Figure 8. IR absorption spectrum of the $H_2O\cdots C_3O$ complex in solid Ar at 9 K in the O−H stretching region. The relevant stretching modes of water are underlined. Monomeric water is present in the sample as an impurity.

respectively. Thus, the complexation-induced shifts feature strong intermolecular bonding in the $H_2O\cdots C_3O$ complex. This is in agreement with the calculated interaction energies, which are −21 kJ/mol in the $H_2O\cdots C_3O$ complex, −7 kJ/mol in the $H_2O\cdots$CO complex,[37] and −5 kJ/mol in the $H_2O\cdots$O complex.[36]

Further Discussion

1. Formation Mechanism. Several ground-state (S_0) reactions have been computationally studied by Ndip et al.[15]

$$\textit{trans}\text{-HCCCOOH} + h\nu \rightarrow \text{cis-HCCCOOH} \quad (1)$$

$$\textit{cis}\text{-HCCCOOH} + h\nu \rightarrow \text{HCCH} + \text{CO}_2 \quad (2)$$

$$\textit{trans}\text{-HCCCOOH} + h\nu \rightarrow \text{HCCOH} + \text{CO} \quad (3)$$

The lower-energy trans form isomerizes to *c*-PA by an internal rotation around the C−O bond (reaction 1). The computations suggest that *c*-PA produces acetylene by elimination of carbon dioxide via migration of the hydrogen atom of the OH group and simultaneous breaking of the C−C bond (reaction 2).[15] The ground-state trans form can produce ethynol and carbon monoxide directly via a three-center transition state or by a two-step mechanism via a four-center transition state (reaction 3).[15] In our experiments, all of these products were seen, thus supporting the theoretical results. However, the observed formation of C_3O and H_2O cannot be explained by these ground-state reactions.

Irradiation at 193 nm can drive propiolic acid into its excited states, and a number of radical channels involving excited electronic states or a hot ground state after internal conversion are energetically possible, following Kumar et al.[14]

$$\text{HCCCOOH} + h\nu \rightarrow \text{HCCCO} + \text{OH} \quad (4)$$

$$\text{HCCCOOH} + h\nu \rightarrow \text{HCC} + \text{HOCO} \quad (5)$$

$$\text{HCCCOOH} + h\nu \rightarrow \text{H} + \text{CCCOOH} \quad (6)$$

These photolysis channels have been observed in the gas phase,

TABLE 5: Experimental and Computational IR Absorption Spectral Data (in cm^{-1}) for the $C_3O\cdots H_2O$ Complex[a]

	Ar matrix			calcd		
mode	complex	monomers[b]	shift	$C_3O\cdots H_2O$	monomers	shift
C_3O stretch	2248.2	2243.0	5.2	2317.1 (1339)	2314.4 (1278)	2.7
	2245.9		2.9			
	2243.1		0.1			
O—H stretch						
asymm	3704.4	3734.3	−29.9	3946.2 (141)	3981.9 (74)	−35.7
symm	3598.5	3638.0	−39.5	3745.3 (478)	3861.7 (10)	−116.4
HOH bend	−	1589.1	−	1689.8 (39)	1660.4 (66)	29.4

[a] The strongest and observable bands are shown only. The relative absorption intensities (in km/mol) are in parentheses. The ab initio spectra are calculated at the MP2/6-311++G(2d,2p) level. [b] Data from refs 30−33.

Figure 9. Calculated structure of the $H_2O\cdots C_3O$ complex. The bond lengths and angle of the complex are shown in normal font, and the values for the monomeric species are given in italics (the lower numbers). The geometries were calculated at the MP2 level of theory with the 6-311++G(2d,2p) basis set.

the major dissociation pathway being the formation of hydroxyl radical (OH).[14] The other observed channels lead to ethynyl (HCC) and hydrocarboxyl (HOCO) radicals and hydrogen atoms. In our experiments, these radicals were not observed in measurable amounts, because of the low cage-exit probability for molecular products.[1] Actually, the detection of OH radicals (3554 cm^{-1} in solid Ar)[35] is complicated by the overlapping absorption of *t*-PA. The cage-exit probability for hydrogen atoms is also small, and the 3-eV excess energy provides a cage-exit probability of 5% in solid Kr.[38] It follows that various in-cage reactions should be considered, such as

$$HCCCO + OH \rightarrow HCCCOOH \quad (7)$$

$$HO + HCCCO \rightarrow H_2O + C_3O \quad (8)$$

$$HCC + HOCO \rightarrow HCCH + CO_2 \quad (9)$$

$$HCC + HOCO \rightarrow HCC + CO + OH \quad (10)$$

$$HCC + CO + OH \rightarrow HCCOH + CO \quad (11)$$

$$H + CCCOOH \rightarrow C_3O + H_2O \quad (12)$$

It is seen that these reactions yield all of the observed photolysis products. A question remains as to whether the photolysis products are formed in the excited or ground state. Another question concerns the role of the precursor conformation for the photolysis channels. For example, it has been found computationally that the ground-state formations of acetylene and ethynol are structurally related to different conformers.[15] The experimental study of these interesting questions is beyond the scope of the present work.

2. Photolysis Kinetics. Figure 10 presents the 193-nm photolysis kinetics of propiolic acid and its photolysis products in solid Kr. The photolysis kinetics results are qualitatively similar in various matrixes. The relative concentration of *c*-PA was found from the tunneling conversion. The relative concentrations of the formed complexes were calculated using the computational absorption intensities of the characteristic bands (the O—H and C—H stretching modes). This approach is limited by the accuracy of the calculated intensities and effect of the matrix on the absorption intensities; however, it still provides

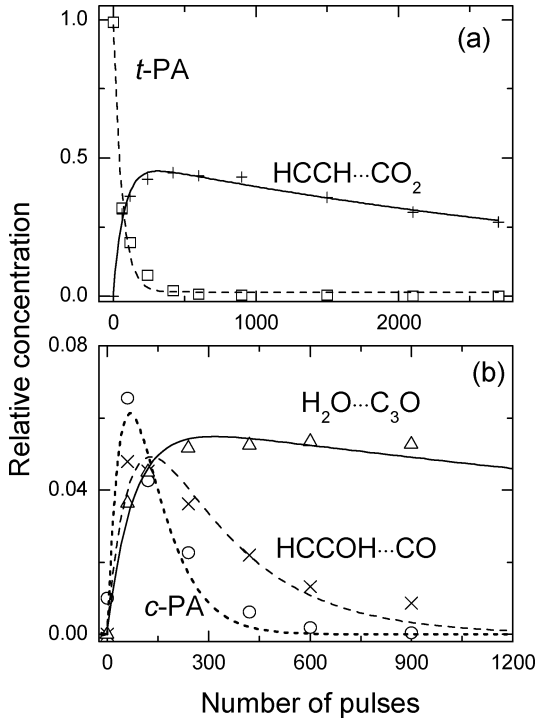

Figure 10. Kinetics of photolysis at 193 nm of propiolic acid in solid Kr at 9 K. Shown are the data for *trans*-propiolic acid (□), *cis*-propiolic acid (○), $HCCH\cdots CO_2$ (+), $HCCOH\cdots CO$ (×), and $H_2O\cdots C_3O$ (Δ). The photolysis was performed with a pulse energy density of ∼10 mJ/cm^2.

a rough idea about the photolysis kinetics. The *c*-PA-to-*t*-PA tunneling conversion occurring during photolysis and the exclusion of some photodecomposition channels from consideration also contribute to the quantitative limitation of this kinetic scheme. For instance, the cage exit of an H atom can lead to the formation of the $CO\cdots CCOH$ complex, with is supported by the observed bands at 2019, 2023, and 2026 cm^{-1}.[39] The photolysis-induced band at 1867 cm^{-1} in solid Ar can be attributed to HCO (the monomer absorbs at 1863 cm^{-1}),[40] which also features additional channels. Finally, the photolysis kinetics is corrupted in optically thick matrixes.[41]

The dominating photolysis product is the $H_2C_2\cdots CO_2$ complex, and it can constitute about one-half of the products. This species can be formed in the ground electronic state (reaction 2) and in the in-cage radical reaction (reaction 9). The bands of the $H_2C_2\cdots CO_2$ complex slowly bleach upon prolonged irradiation, probably as a result of the photodecomposition of acetylene reported in noble-gas solids.[25] This photodecomposition can lead to the cage exit of H atoms and/or to the in-cage formation of HOCO, which has a calculated reaction barrier of 1.2 eV.[42] The $CO\cdots HCCOH$ complex is not observed in large amounts; however, its formation is rather efficient, even though several

times less efficient compared to the $H_2C_2\cdots CO_2$ complex. The $CO\cdots HCCOH$ concentration is essentially limited by the efficient photodecomposition of this species, which is about 4 times faster than that of the $H_2C_2\cdots CO_2$ complex in solid Ar. The $H_2O\cdots C_3O$ complex reaches minor concentrations even though it is quite photostable, which means that it is formed quite inefficiently (an order of magnitude less efficiently than $H_2C_2\cdots CO_2$). This last product is formed in radical reactions that require excitation to the upper electronic states, whereas the first two products can be formed in the ground state, highlighting the likely importance of ground-state reactions in the photolysis of propiolic acid in noble-gas solids.

Concluding Remarks

We have studied the 193-nm photolysis of propiolic acid (HCCCOOH) in noble-gas (Ar, Kr, and Xe) matrixes. The photolysis products were assigned using Fourier transform infrared spectroscopy and ab initio quantum chemistry calculations. Four distinct photolysis products were found. First, the higher-energy cis conformer of propiolic acid was efficiently formed upon irradiation and decayed back to the trans form on a time scale of ~10 min by tunneling of the hydrogen atom through the torsional energy barrier. This conformer of propiolic acid was observed for the first time. It is an unusual case in which a conformer of a small carboxylic acid that is unstable with respect to rotation about a single C—O bond is obtained using UV photolysis of the stable form. More often, the higher-energy forms of small carboxylic acids have been prepared with infrared pumping.[9] However, the conformational process promoted by UV light was reported for oxalic acid.[6]

In addition, the photolysis produced three well-defined molecular complexes of the forms $HCCH\cdots CO_2$, $HCCOH\cdots CO$, and $H_2O\cdots C_3O$. These species can be formed in the ground state and via radical reactions promoted by the strong cage effect of a solid matrix. The $HCCH\cdots CO_2$ complex dominated over the photolysis products, with calculations suggesting the parallel geometry of this complex. The formation rate of the $HCCOH\cdots CO$ complex was also rather high, but its concentration was strongly limited by the efficient light-induced decomposition. In this complex, the most probable geometry involves the binding of carbon monoxide to the OH group via the carbon atom, with a calculated interaction energy of −18.3 kJ/mol. The other complex structure interacting via the CH group was not detected experimentally, and its calculated interaction energy was quite small (−6.4 kJ/mol). The formation of the relatively strong $H_2O\cdots C_3O$ complex (interaction energy −21 kJ/mol) was less efficient, which might be due to the inefficiency of the involved radical reaction.

The identification of the molecular complexes was quite straightforward experimentally; however, in some cases, discrepancies between experimental and theoretical vibrational spectra arose, and these should be noted. For instance, this is the case for the complex between ethynol and carbon monoxide. We assigned the observed absorption to two sites of the $HCCOH\cdots CO$ complex geometry in which carbon monoxide is bonded to the OH group via the carbon atom, although some discrepancy between the experimental and theoretical shifts was found. On the other hand, our structural analysis was essentially based on the literature data of HCCOH monomer,[20] which makes our structural discussion rather conditional. As a general reason for numerical disagreements between experiment and theory, the calculations were performed for the interacting pair in a vacuum, whereas the experimental species were isolated in a solid host. The original cage might be too tight for the photolysis products,[43] and this can influence the complex geometry. Furthermore, the reference monomeric species were studied in solid matrixes, so that their vibrational spectra were changed by the matrix effect (solvation), which can be comparable to a complexation-induced shift, hence further complicating the analysis.[44] Finally, it seems that the theory employed cannot precisely reproduce the complexation-induced shifts, which makes the confident determination of complex geometries difficult. For instance, this is seen for the C—H stretching mode of the $HCCH\cdots CO_2$ complex, where the calculation of the parallel complex geometry gives a shift of $-2.1\ cm^{-1}$, which differs from the value reported for this complex in the gas phase ($-8\ cm^{-1}$).[16]

Acknowledgment. The Academy of Finland supported this work. We thank H. Tanskanen and S. Johansson for additional experimental data in solid Xe and E. Maçôas for important discussions.

Note Added after ASAP Publication. This paper was published ASAP on September 21, 2006. A footnote in Table 5 was changed. The updated paper was reposted on September 27, 2006.

References and Notes

(1) Apkarian, V. A.; Schwentner, N. *Chem. Rev.* **1999**, *99*, 1481.
(2) Lundell, J.; Räsänen, M. *J. Mol. Struct.* **1997**, *437*, 349.
(3) Khriachtchev, L.; Maçôas, E. M. S.; Pettersson, M.; Räsänen, M. *J. Am. Chem. Soc.* **2002**, *124*, 10994.
(4) Maçôas, E. M. S.; Khriachtchev, L.; Fausto, R.; Räsänen, M. *J. Phys. Chem. A* **2004**, *108*, 3380.
(5) Hall, R. T.; Pimentel, G. C. *J. Chem. Phys.* **1963**, *38*, 1889.
(6) Nieminen, J.; Räsänen, M.; Murto, J. *J. Phys. Chem.* **1992**, *96*, 5303.
(7) Khriachtchev, L.; Lundell, J.; Isoniemi, E.; Räsänen, M. *J. Chem. Phys.* **2000**, *113*, 4265.
(8) Pettersson, M.; Lundell, J.; Khriachtchev, L.; Räsänen, M. *J. Am. Chem. Soc.* **1997**, *119*, 11715.
(9) Maçôas, E. M. S.; Khriachtchev, L.; Pettersson, M.; Fausto, R.; Räsänen, M. *Phys. Chem. Chem. Phys.* **2005**, *7*, 743.
(10) Maçôas, E. M. S.; Khriachtchev, L.; Pettersson, M.; Juselius, J.; Fausto, R.; Räsänen, M. *J. Chem. Phys.* **2003**, *119*, 11765.
(11) Pettersson, M.; Maçôas, E. M. S.; Lundell, J.; Khriachtchev, L.; Fausto, R.; Räsänen, M. *J. Chem. Phys.* **2002**, *117*, 9095.
(12) Katon, J. E.; McDevitt, N. T. *Spectrochim. Acta* **1965**, *21*, 1717.
(13) Ndip, E. M. N. Vibrational analysis and ab initio studies of propiolic acid. Ph.D. Thesis, Texas Tech University, Lubbock, TX, 1987.
(14) Kumar, A.; Upadhyaya, H. P.; Naik, P. D.; Maity, D. K.; Mittal, J. P. *J. Phys. Chem. A* **2002**, *106*, 11847.
(15) Ndip, E. M. N.; Shukla, M. K.; Leszczynski, J.; Redington, R. L. *Int. J. Quantum Chem.* **2004**, *100*, 779.
(16) Prichard, D. G.; Nandi, R. N.; Muenter, J. S.; Howard B. J. *J. Chem. Phys.* **1988**, *89*, 1245.
(17) De Almeida, W. B. *Chem. Phys.* **1990**, *141*, 297.
(18) Huang, Z. S.; Miller, R. E. *Chem. Phys.* **1989**, *132*, 185.
(19) Hochstrasser, R.; Wirz, J. *Angew. Chem., Int. Ed. Engl.* **1989**, *28*, 181.
(20) Hochstrasser, R.; Wirz, J. *Angew. Chem., Int. Ed. Engl.* **1990**, *29*, 411.
(21) DeFrees, D. J.; McLean, A. D. *J. Phys. Chem.* **1982**, *86*, 2835.
(22) Dommen, J.; Rodler, M.; Ha, T.-K. *Chem. Phys.* **1987**, *117*, 65.
(23) (a) Frisch, M. J.; Trucks, G. W.; Schlegel, H. B.; Scuseria, G. E.; Robb, M. A.; Cheeseman, J. R.; Zakrzewski, V. G.; Montgomery, J. A., Jr.; Stratmann, R. E.; Burant, J. C.; Dapprich, S.; Millam, J. M.; Daniels, A. D.; Kudin, K. N.; Strain, M. C.; Farkas, O.; Tomasi, J.; Barone, V.; Cossi, M.; Cammi, R.; Mennucci, B.; Pomelli, C.; Adamo, C.; Clifford, S.; Ochterski, J.; Petersson, G. A.; Ayala, P. Y.; Cui, Q.; Morokuma, K.; Malick, D. K.; Rabuck, A. D.; Raghavachari, K.; Foresman, J. B.; Cioslowski, J.; Ortiz, J. V.; Stefanov, B. B.; Liu, G.; Liashenko, A.; Piskorz, P.; Komaromi, I.; Gomperts, R.; Martin, R. L.; Fox, D. J.; Keith, T.; Al-Laham, M. A.; Peng, C. Y.; Nanayakkara, A.; Gonzalez, C.; Challacombe, M.; Gill, P. M. W.; Johnson, B. G.; Chen, W.; Wong, M. W.; Andres, J. L.; Head-Gordon, M.; Replogle, E. S.; Pople, J. A. *Gaussian 98*, revision A.11; Gaussian, Inc.: Pittsburgh, PA, 1998. (b) Frisch, M. J. Trucks, G. W.; Schlegel, H. B.; Scuseria, G. E.; Robb, M. A.; Cheeseman, J. R.; Montgomery, J. A., Jr.; Vreven, T.; Kudin, K. N.; Burant, J. C.; Millam, J. M.; Iyengar, S. S.;

Tomasi, J.; Barone, V.; Mennucci, B.; Cossi, M.; Scalmani, G.; Rega, N.; Petersson, G. A.; Nakatsuji, H.; Hada, M.; Ehara, M.; Toyota, K.; Fukuda, R.; Hasegawa, J.; Ishida, M.; Nakajima, T.; Honda, Y.; Kitao, O.; Nakai, H.; Klene, M.; Li, X.; Knox, J. E.; Hratchian, H. P.; Cross, J. B.; Bakken, V.; Adamo, C.; Jaramillo, J.; Gomperts, R.; Stratmann, R. E.; Yazyev, O.; Austin, A. J.; Cammi, R.; Pomelli, C.; Ochterski, J. W.; Ayala, P. Y.; Morokuma, K.; Voth, G. A.; Salvador, P.; Dannenberg, J. J.; Zakrzewski, V. G.; Dapprich, S.; Daniels, A. D.; Strain, M. C.; Farkas, O.; Malick, D. K.; Rabuck, A. D.; Raghavachari, K.; Foresman, J. B.; Ortiz, J. V.; Cui, Q.; Baboul, A. G.; Clifford, S.; Cioslowski, J.; Stefanov, B. B.; Liu, G.; Liashenko, A.; Piskorz, P.; Komaromi, I.; Martin, R. L.; Fox, D. J.; Keith, T.; Al-Laham, M. A.; Peng, C. Y.; Nanayakkara, A.; Challacombe, M.; Gill, P. M. W.; Johnson, B.; Chen, W.; Wong, M. W.; Gonzalez, C.; Pople, J. A. *Gaussian 03*, revision C.02; Gaussian, Inc.: Pittsburgh, PA, 2003.

(24) (a) Andrews, L.; Johnson, G. L.; Kelsall, B. J. *J. Phys. Chem.* **1982**, *86*, 3374. (b) Engdahl, A.; Nelander, B. *Chem. Phys. Lett.* **1983**, *100*, 129.

(25) Tanskanen, H.; Khriachtchev, L.; Lundell, J.; Räsänen, M. *J. Chem. Phys.* **2004**, *121*, 8291.

(26) Irvine, M. J.; Mathieson, J. G.; Pullin, A. D. E. *Aust. J. Chem.* **1982**, *35*, 1971.

(27) Vigasin, A. A.; Schriver-Mazzuoli, L.; Schriver, A. *J. Phys. Chem. A* **2000**, *104*, 5451.

(28) Dubost, H.; Abouaf-Marguin, L. *Chem Phys. Lett.* **1972**, *17*, 269.

(29) Romano, R. M.; Vedova, C. O. D.; Downs, A. J. *J. Phys. Chem. A* **2002**, *106*, 7235.

(30) Engdahl, A.; Nelander, B. *J. Mol. Struct.* **1989**, *193*, 101.

(31) DeKock, R. L.; Weltner, W., Jr. *J. Am. Chem. Soc.* **1971**, *93*, 7106.

(32) Brown, R. D.; Pullin, D. E.; Rice, E. H. N.; Rodler, M. *J. Am. Chem. Soc.* **1985**, *107*, 7877.

(33) Botschwina, P.; Reisenauer, H. P. *Chem. Phys. Lett.* **1991**, *183*, 217.

(34) Khriachtchev, L.; Tanskanen, H.; Pettersson, M.; Räsänen M.; Ahokas, J.; Kunttu. H.; Feldman, V. *J. Chem. Phys.* **2002**, *116*, 5649.

(35) Khriachtchev, L.; Pettersson, M.; Tuominen, S.; Räsänen, M. *J. Chem. Phys.* **1997**, *107*, 7252.

(36) Pehkonen, S.; Pettersson, M.; Lundell, J.; Khriachtchev, L.; Räsänen, M. *J. Phys. Chem. A* **1998**, *102*, 7643.

(37) Lundell, J.; Latajka, Z. *J. Phys. Chem. A* **1997**, *101*, 5004.

(38) Dickgiesser, M.; Schwentner, N. *Nucl. Instrum. Methods Phys. Res. B* **2000**, *168*, 252.

(39) Jacox, M. E.; Olson, W. B. *J. Chem. Phys.* **1987**, *86*, 3134.

(40) Milligan, D. E.; Jacox, M. E. *J. Chem. Phys.* **1969**, *51*, 277.

(41) Khriachtchev, L.; Pettersson, M.; Räsänen, M. *Chem. Phys. Lett.* **1998**, *288*, 727.

(42) Setzler, J. V.; Behtel, J.; Guo, H.; Schatz, G. C. *J. Chem. Phys.* **1997**, *107*, 9176.

(43) Engdahl, A.; Nelander, B. *Phys. Chem. Chem. Phys*. **2002**, *4*, 2140.

(44) Lundell, J.; Jolkkonen, S.; Khriachtchev, L.; Pettersson, M.; Räsänen, M. *Chem. Eur. J.* **2001**, *7*, 1670.